Supplement of Earth Surf. Dynam., 8, 769–787, 2020
https://doi.org/10.5194/esurf-8-769-2020-supplement

Supplement of

Timing of exotic, far-traveled boulder emplacement and paleo-outburst flooding in the central Himalayas

Marius L. Huber et al.

Correspondence to: Marius L. Huber (marius.huber@univ-lorraine.fr)

Supplement 1 (S1): Field survey and boulder provenance

S1.1 Overview maps of field sites

Samples on tributary fan, south of Devighat, "Trishuli downstream"
Sampled boulders: NEQ/162 **44**, …**45**, …**46** and …**47**
Many boulders spread on a tributary fan at the Trishuli River, south of Devighat

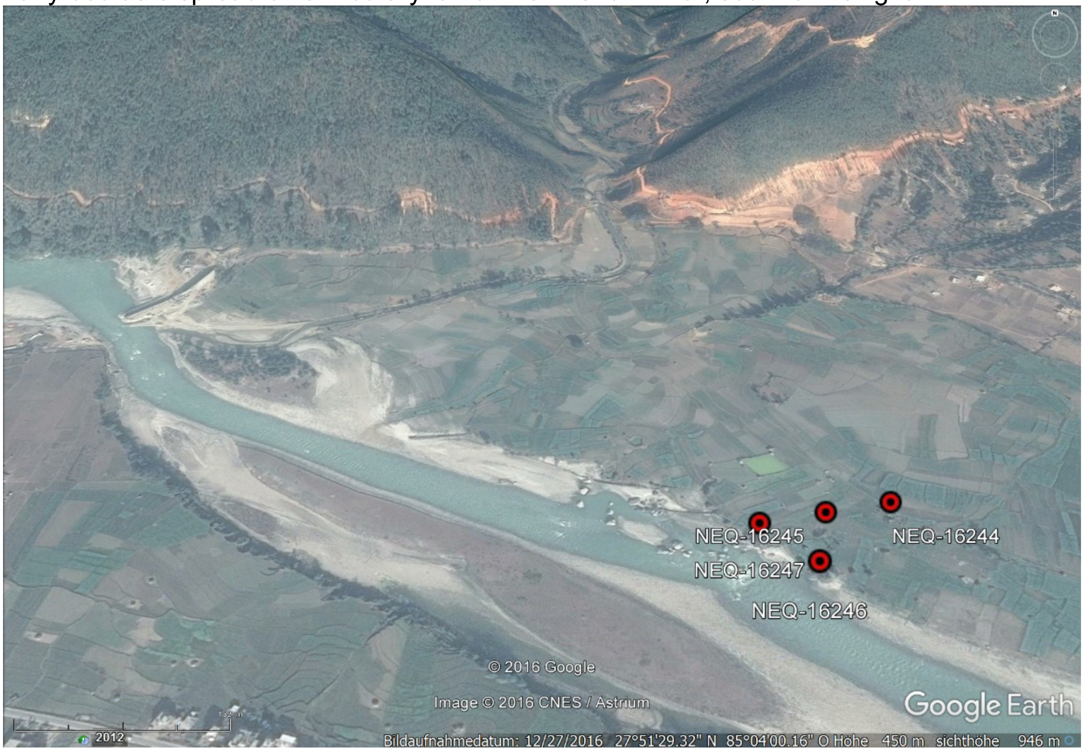

Figure S1.1-1: Google Earth, n. d., [satellite imagery for central Nepal], Retrieved June to November 2017, Google Earth Version 7.3.0

Samples at fill terrace, Betrawati, “Trishuli upstream”
Sampled boulders: NEQ/162 **60**, …**61**, …**66** and …**67**.

Figure S1.1-2: Google Earth, n. d., [satellite imagery for central Nepal], Retrieved June to November 2017, Google Earth © 2016 DigitalGlobe

Samples north of Betrawati "Trishuli upstream"
Sampled boulders: NEQ/162 **58**, and …**59**.

Figure S1.1-3:Google Earth, n. d., [satellite imagery for central Nepal], Retrieved June to November 2017, Google Earth © 2016 DigitalGlobe

Samples around Balephi, Sunkoshi/ Balephi Khola
Sampled boulders: NEQ/161 **01**, …**02** and …**03.** And NEQ/162 **79**, …**80** and …**98**.

Figure S1.1-4: Google Earth, n. d., [satellite imagery for central Nepal], Retrieved January 2020, Google Earth © 2020 CNES/Airbus

S1.2 Sampled boulders in detail

- **NEQ/162 44** (“Trishuli downstream”)


Figure S1.2-1


Figure S1.2-2

Orthogneiss of Higher Himalayan origin.

- **NEQ/162 45** ("Trishuli downstream")


Figure S1.2-3


Figure S1.2-4

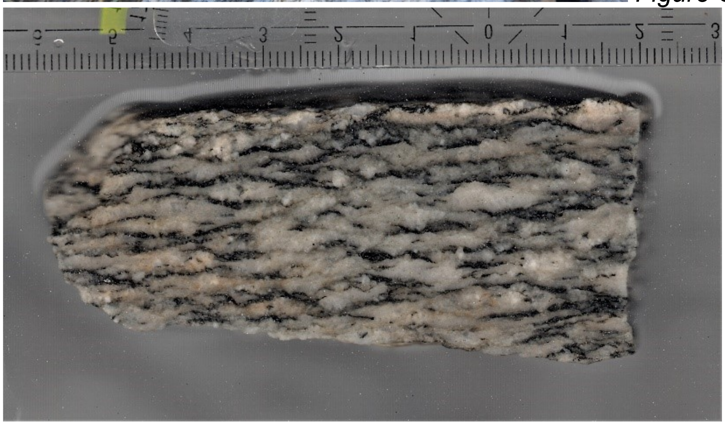
Figure S1.2-5

Orthogneiss of Higher Himalayan origin.

- **NEQ/162 46** ("Trishuli downstream")

Figure S1.2-6

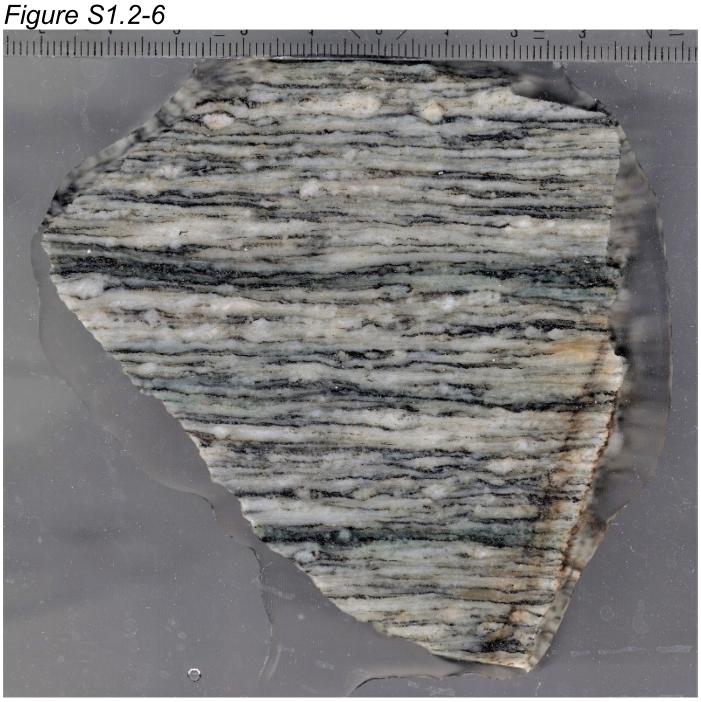

Figure S1.2-7

Orthogneiss of Higher Himalayan origin.

- **NEQ/162 47** (“Trishuli downstream”)

Figure S1.2-8

Figure S1.2-9

Phyllitic schist of Lesser Himalayan sequence, most likely Kuncha Formation within Nawakot Complex, Dandagaon Formation could also be possible.

- **NEQ/162 58** (“Trishuli upstream”)

Figure S1.2-10

Figure S1.2-11

Figure S1.2-12

Figure S1.2-13

Figure S1.2-14

Phyllite of Lesser Himalayan sequence, most likely Kuncha Formation within Nawakot Complex, Dandagaon Formation could also be possible.

- **NEQ/162 59** ("Trishuli upstream")

Figure S1.2-15

Figure S1.2-16

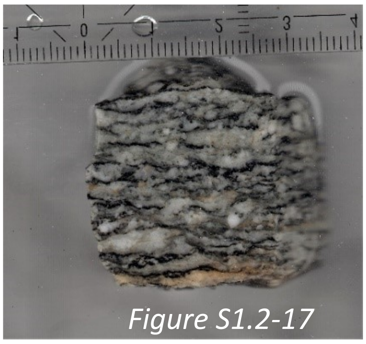

Figure S1.2-17

Figure S1.2-18

Orthogneiss of Higher Himalayan origin.

- **NEQ/162 60** ("Trishuli upstream")

Figure S1.2-19

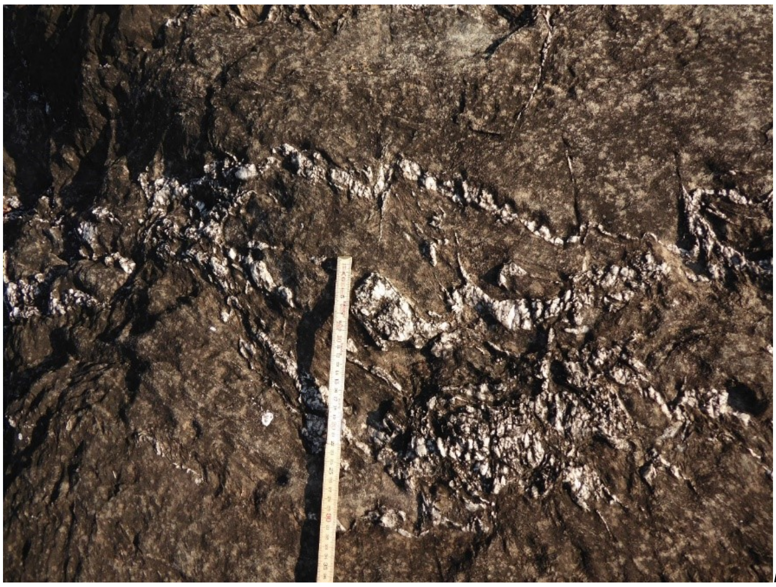

Figure S1.2-20

Schist of Lesser Himalayan sequence, most likely Kuncha Formation within Nawakot Complex Dandagaon Formation could also be possible.

- **NEQ/162 61** (“Trishuli upstream”)


Figure S1.2-21


Figure S1.2-22

Schist of Lesser Himalayan sequence, most likely Kuncha Formation within Nawakot Complex, Dandagaon Formation could also be possible.

- **NEQ/162 66** (“Trishuli upstream”)

Figure S1.2-23

Figure S1.2-24

Figure S1.2-25

Schist of Lesser Himalayan sequence, most likely Kuncha Formation within Nawakot Complex, Dandagaon Formation could also be possible.

- **NEQ/162 67** ("Trishuli upstream")

Figure S1.2-26

Figure S1.2-27

Figure S1.2-28

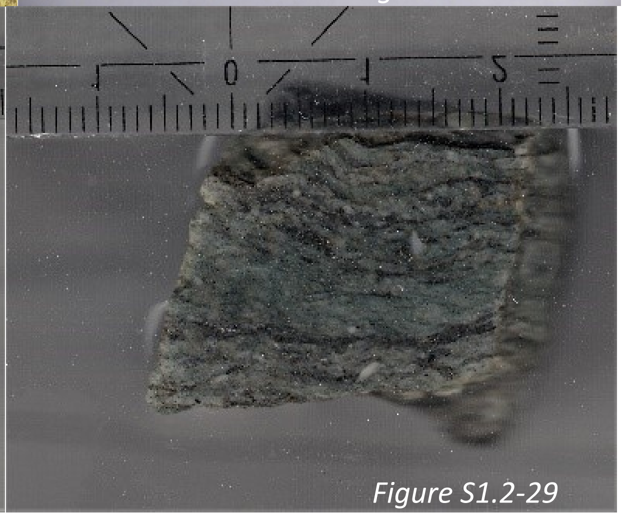

Figure S1.2-29

Phyllitic schist of Lesser Himalayan sequence, most likely Kuncha Formation within Nawakot Complex, Dandagaon Formation could also be possible. Different fabric than 47, 58, 60, 61 and 66.

- **NEQ-161 01** (Sunkoshi)

Figure S1.2-30

Figure S1.2-31

Orthogneiss of Higher Himalayan Crystallines (no Lesser Himalayan sequence), with garnets, maybe with leucosomes, migmatitic, too homogenous for a paragneiss.

- **NEQ/161 02** (Sunkoshi)

Figure S1.2-32

Figure S1.2-33

Figure S1.2-34

whitish orthogneiss of undifferentiated Higher Himalayan Crystallines (no lesser Himalayan sequence), no garnet found.

- **NEQ/161 03** (Sunkoshi)


Figure S1.2-35


Figure S1.2-36


Figure S1.2-37

Augengneiss, likely Ulleri-gneiss of Lesser Himalayan sequence, outcrops only just below the MCT in the study region, no intrusions mapped or known to the authors which are located south of these areas (Shrestha et al., 1986; Dhital, 2015), with garnets.

- **NEQ/162 79** (Sunkoshi, Balephi Khola)


Figure S1.2-38


Figure S1.2-39

Augengneiss, possibly metagranitoide, of Higher Himalayan Crystallines (no Lesser Himalayan sequence)

- **NEQ/162 80** (Sunkoshi)

Figure S1.2-40

Figure S1.2-41

Figure S1.2-42

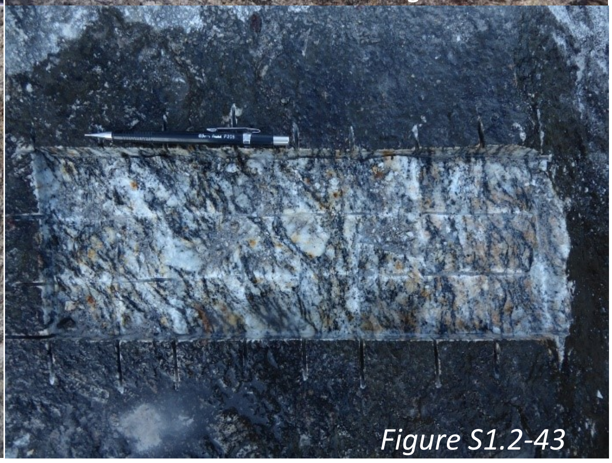

Figure S1.2-43

Augengneiss of Higher Himalayan Crystallines (no Lesser Himalayan sequence), structure quite common in the Higher Himalayan Crystallines.

- **NEQ/162 98** (Sunkoshi, Balephi Khola)

Figure S1.2-44

Figure S1.2-45

Augengneiss of Higher Himalayan Crystallines (no Lesser Himalayan sequence), structure quite common in the Higher Himalayan Crystallines.

S1.3 Fill-terraces at Betrawati and further downstream

Figure S1.3-A:
Coordinates of viewpoint:
27.96925, 85.18104
Betrawati fill-terrace at river-cut seen from different angle than Figure 2B. Deposit has sorting, some grading and clast-supported texture. Surveyed boulder NEQ/162 66 with intermediate diameter of 8.8 m sitting on top. Photo credit K. Cook, GFZ Potsdam - 2017).

Figure S1.3-B:
Coordinates of viewpoint:
27.95223, 85.16403
Large boulder (probably >10 m maximum diameter) spotted half-buried in fill-deposit approx. 3 km south of Betrawati terrace and "Trishuli upstream" boulders. Excavation of boulder after deposition by river incision likely (river behind utility pole).

Figure S1.3-C:
Coordinates of viewpoint:
27.94721, 85.16353
Boulder of B seen from other angle (in red circle). Hydropower facility in the foreground.

Supplement 2 (S2): Paleo-hydrologic discharge estimation

Topographic maps used for river channel cross-section extraction

Topo-maps by the Government of Nepal, Survey Department produced in co-operation with the Government of Finland and the Finnish Meteorological Institute.

Following map sheets are covering the study are and were utilised for channel cross-section extraction (including scale and year of publication):
2785 01B Nuwakot, 1 : 25 000, 1996 (20 m contour spacing)
2785 01C Devighat, 1 : 25 000, 1996 (20 m contour spacing)
2785 04 Barhabise, 1 : 50 000, 1996 (40 m contour spacing)
2785 08 Dadapakhar, 1 : 50 000, 1996 (40 m contour spacing)
2885 13 Somdan, 1 : 50 000, 1997 (40 m contour spacing)

Cross-section site selecting was done with guidelines by Costa (1983), p.997.

Profiles were drawn with Matlab-function "manningseq" in supplementary material from Rosenwinkel et al. (2017), by Schwanghart.

Parameters, imported data and results generated with "bouldersforpaleohydrology" code-package (Matlab) accessible via URL https://gitlab.com/mlh300/bouldersforpaleohydrology/

Basic parameters used for code allochthonous_boulders_for_paleohydrology.m

Flood water density: **rho_f = 1500** kg/m^3
Gravitational acceleration: **g = 9.81** m/s^2

Basic parameters used for function manningseq.m

Manning's roughness coefficient for mountain streams (Chow, 1959): **n = 0.04** s/(m^(1/3))
("manningseq" in supplementary material from Rosenwinkel et al. (2017), by Schwanghart)

Input data for code allochthonous_boulders_for_paleohydrology.m

Table S2-1: Boulders import table:

sample name	intermediate diameter [m]	density of boulder rock material [kg/m^3]	topoprofiles
NEQ/161 01	8.7	2800	11,12
NEQ/161 02	4.5	2800	11,12
NEQ/161 03	29.9	2800	11,12
NEQ/162 44	9.2	2800	6,7
NEQ/162 45	9.9	2800	6,7
NEQ/162 46	12.5	2800	6,7
NEQ/162 47	18	2700	6,7
NEQ/162 58	13.4	2700	1,2
NEQ/162 59	8.5	2800	1,2
NEQ/162 60	18.6	2700	3,4
NEQ/162 61	14.7	2700	3,4
NEQ/162 66	8.8	2700	3,4
NEQ/162 67	9.9	2700	3,4
NEQ/162 79	9.5	2800	9,10
NEQ/162 80	11.4	2800	9,10
NEQ/162 98	9.4	2800	9,10

Table S2-2.1: Topoprofile import table (1), d and z in meter, S in rad

topo1			topo2			topo3			topo4			topo5		
28°02’07.01’’N, 85°11’38.72’’E			28°00’26.87’’N, 85°11’00.67’’E			27°59'12.22"N, 85°10'48.65"E			27°58'41.48"N, 85°10'54.34"E			27°58'12.08"N, 85°10'53.10"E		
d_1	z_1	S_1	d_2	z_2	S_2	d_3	z_3	S_3	d_4	z_4	S_4	d_5	z_5	S_5
0	1000	0.0242	0	1000	0.0251	0	880	0.0174	0	800	0.0115	0	800	0.0155
38.5	960		96.2	960		35	860		42	780		35	780	
57.7	920		173.1	920		90.9	840		70	760		104.9	760	
105.8	880		221.2	880		167.8	820		90.9	740		188.8	740	
173.1	840		288.5	840		216.8	800		118.9	720		230.8	720	
221.2	800		326.9	800		244.8	780		139.9	700		280	700	
278.8	765		355.8	760		293.7	760		153.8	680		580.4	680	
432.7	765		384.6	720		321.7	740		167.8	660		594.4	660	
461.5	800		451.9	680		370.6	720		188.8	640		615.4	640	
509.6	840		461.5	675		398.6	700		286.7	620		832.2	620	
557.7	880		538.5	675		426.6	680		328.7	612		937.1	613	
596.2	920		605.8	680		454.5	660		398.6	612		958	600	
634.6	960		730.8	720		482.5	640		426.6	620		965	593	
663.5	1000		788.5	760		496.5	620		503.5	640		1035	593	
			846.2	800		503.5	619		531.5	660		1055.9	600	
			894.2	840		545.5	619		566.4	680		1167.8	620	
			971.2	880		566.4	620		601.4	700		1216.8	640	
			1057.7	920		762.2	640		713.3	720		1244.8	660	
						839.2	660		762.2	740		1265.7	680	
						860.1	680		797.2	760		1293.7	700	
						881.1	700		832.2	780		1328.7	720	
						909.1	720		909.1	800		1363.6	740	
						972	740					1391.6	760	
						1007	760					1419.6	780	
						1049	780					1440.6	800	
						1076.9	800							
						1104.9	820							

Table S2-2.2: Topoprofile import table (2), d and z in meter, S in rad

topo6			topo7			topo8			topo9			topo10		
27°51'36.29"N, 85° 5'43.84"E			27°51'25.16"N, 85°5'16.79"E			27°51'21.20"N, 85° 4'4.40"E			27°44'41.99"N, 85°46'39.96"E			27°44'24.34"N, 85°46'41.10"E		
d_6	z_6	S_6	d_7	z_7	S_7	d_8	z_8	S_8	d_9	z_9	S_9	d_10	z_10	S_10
0	600	0.004	0	700	0.004	0	700	0.003	0	1000	0.01	0	1000	0.01
37.5	580		49.6	680		42.6	680		85.6	960		58.8	960	
90.4	560		78	660		120.6	660		128.3	920		96.3	920	
122.3	540		127.7	640		156	640		171.1	880		155.1	880	
154.3	520		177.3	620		177.3	620		208.6	840		187.2	840	
276.6	500		212.8	600		269.5	600		262	800		240.6	800	
446.8	480		241.1	580		354.6	580		320.9	760		283.4	760	
946.8	460		290.8	560		383	560		417.1	720		331.6	720	
989.4	453		390.1	540		404.3	540		475.9	692		406.4	695	
1143.6	453		723.4	520		446.8	520		524.1	692		459.9	695	
1149	460		808.5	520		489.4	500		545.5	720		492	720	
1303.2	480		879.4	520		517.7	480		609.6	760		545.5	760	
1590.4	500		1007.1	500		567.4	460		657.8	800		620.3	800	
1712.8	520		1113.5	480		1056.5	441.5		732.6	840		668.4	840	
1840.4	540		1163.1	460		1361.7	441.5		791.4	880		727.3	880	
1888.3	560		1290.8	450		1510.6	460		866.3	920		839.6	920	
1925.5	580		1418.4	450		1730.5	480		909.1	960		957.2	960	
1968.1	600		1609.9	460		1808.5	500		973.3	1000		1026.7	1000	
			1666.7	480		1971.6	520							
			1716.31	500		2078	540							
			1844	520		2163.1	560							
			1907.8	540		2205.7	580							
			1943.3	560		2262.4	600							
			2021.3	580		2283.7	620							
			2099.3	600		2319.1	640							
			2170.2	620		2390.1	660							
			2212.8	640		2432.6	680							
			2262.4	660		2496.5	700							
			2333.3	680										
			2439.7	700										

Table S2-2.3: Topoprofile import table (3), d and z in meter, S in rad

topo11			topo12			topo13		
27°43'44.73"N, 85°46'45.76"E			27°43'41.55"N, 85°46'44.38"E			27°43'28.60"N, 85°46'41.86"E		
d_11	z_11	S_11	d_12	z_12	S_12	d_13	z_13	S_13
0	1000	0.006	0	1000	0.006	0	1000	0.006
48.5	960		69.5	960		213.9	960	
90.9	920		128.3	920		534.8	920	
171.1	880		197.9	880		625.7	880	
240.6	840		235.3	840		673.8	840	
294.1	800		320.9	800		850.3	800	
342.2	760		390.4	760		898.4	760	
395.7	720		443.9	720		935.8	720	
449.2	680		513.4	680		1048.1	680	
459.9	671		540.1	670		1069.5	667	
545.5	671		609.6	670		1144.4	667	
550.8	680		625.7	680		1155.1	680	
582.9	720		668.4	720		1326.2	720	
636.4	760		695.2	760		1417.1	760	
684.5	800		743.3	800		1470.6	800	
738	840		780.7	840		1679.1	840	
812.8	880		850.3	880		1802.1	880	
844.9	920		898.4	920		1844.9	920	
903.7	960		984	960		1909.1	960	
973.3	1000		1155.1	1000		1978.6	1000	

Output data from code allochthonous_boulders_for_paleohydrology.m

Table S2-3: Paleohydrology results from boulders

				Flow velocity [m/s]			Flow discharge [m3/s]			Flow height [m]		
sample name	boulder diameter [m]	density of boulder rock material [kg/m^3]	topoprofiles used for calculation	Costa (1983)	Clarke (1996)	Alexander& Cooker (2016)	Costa (1983)	Clarke (1996)	Alexander& Cooker (2016)	Costa (1983)	Clarke (1996)	Alexander& Cooker (2016)
NEQ/161 01	8.7	2800	11,12	10.2	9.3	6.0	1.64E+04	1.25E+04	3.39E+03	15.9	13.7	6.4
NEQ/161 02	4.5	2800	11,12	7.8	6.7	4.3	7.29E+03	4.62E+03	1.34E+03	10.0	7.7	3.7
NEQ/161 03	29.9	2800	11,12	16.7	17.3	11.2	8.95E+04	1.03E+05	2.25E+04	40.5	43.6	19.0
NEQ/162 44	9.2	2800	6,7	10.4	9.6	6.2	1.31E+05	1.02E+05	2.13E+04	27.2	24.5	12.6
NEQ/162 45	9.9	2800	6,7	10.7	10.0	6.4	1.44E+05	1.15E+05	2.44E+04	28.3	25.7	13.4
NEQ/162 46	12.5	2800	6,7	11.8	11.2	7.2	1.97E+05	1.69E+05	3.74E+04	32.2	30.2	16.1
NEQ/162 47	18	2700	6,7	13.6	12.9	8.3	3.27E+05	2.74E+05	6.19E+04	40.1	37.1	20.0
NEQ/162 58	13.4	2700	1,2	12.1	10.8	7.2	1.10E+04	8.16E+03	2.56E+03	6.4	5.4	2.8
NEQ/162 59	8.5	2800	1,2	10.1	9.0	6.0	6.74E+03	4.85E+03	1.53E+03	4.9	4.1	2.1
NEQ/162 60	18.6	2700	3,4	13.8	12.9	8.5	3.11E+04	2.47E+04	5.39E+03	16.0	14.3	6.6
NEQ/162 61	14.7	2700	3,4	12.5	11.5	7.5	2.19E+04	1.60E+04	3.63E+03	13.5	11.5	5.4
NEQ/162 66	8.8	2700	3,4	10.2	8.9	5.8	1.04E+04	6.43E+03	1.60E+03	9.3	7.2	3.4
NEQ/162 67	9.9	2700	3,4	10.7	9.4	6.2	1.23E+04	7.89E+03	1.92E+03	10.1	8.1	3.8
NEQ/162 79	9.5	2800	9,10	10.5	9.7	6.3	9.24E+03	6.98E+03	1.80E+03	12.1	10.4	4.8
NEQ/162 80	11.4	2800	9,10	11.3	10.6	6.9	1.19E+04	9.52E+03	2.37E+03	13.9	12.3	5.6
NEQ/162 98	9.4	2800	9,10	10.5	9.6	6.3	9.11E+03	6.86E+03	1.77E+03	12.0	10.3	4.7

Supplement 3 (S3): Boulder exposure ages

Surface exposure dating with cosmogenic nuclides developed substantially in the last two decades and has become a powerful tool in analysing landscape evolution in Quaternary Geology and Geomorphology (e.g. Ivy-Ochs and Kober, 2008). Taking into account local cosmogenic nuclide production and topographic shielding, which lowers production, a surface exposure age is calculated from the cosmogenic nuclide concentrations by solving for t in Equation S3-1 below, where nuclide concentration N [atoms g^{-1}] is given as a function of time t [a] with production rate P [atoms g^{-1} a^{-1}] and decay constant λ [a^{-1}]. Equation S3-1 simplifies the evolution of cosmogenic nuclide concentrations by neglecting inheritance and erosion. Following standard chemical separation procedures (details provided below), concentrations of cosmogenic nuclides are measured with accelerated mass spectrometry (AMS). The radionuclide ^{10}Be ($^{16}O(n,4p3n)^{10}Be$) is used in this study for cosmogenic nuclide dating because the target mineral quartz (SiO_2) is abundant in the sampled lithologies. Exposure dating with ^{10}Be is a well-established method, comparably easy to apply and delivers reliable results for the targeted time-frame (Dunai, 2010).

$$N(t) = \frac{P}{\lambda} \times (1 - e^{-\lambda t}) \qquad \text{(S3-1)}$$

Laboratory work

Sample preparation was performed in the laboratories of the Geological Institute in the Earth Science Department at ETH Zurich. The procedure employed is based on Ivy-Ochs (1996) with modifications from Norton et al. (2008), which itself is adapted after Von Blanckenburg et al. (1996, 2004). Samples were crushed with high-voltage pulse power fragmentation (SELFRAG), sieved to grain sizes between 1000 μm to 250 μm and magnetically separated to remove unwanted magnetic minerals from each sample. Repetitive acid treatment with diluted hydrochloric (HCL), hexafluorosilicic (H_2SiF_6) and hydrofluoric (HF) acids was used to remove minerals, mainly oxides, carbonates and feldspars from the sample material and isolate quartz (Norton et al. 2008). In order to fully remove meteoric ^{10}Be from the remaining crystals, the grain boundaries of the quartz were leached with HF 3 times so as to dissolve 10% of the quartz mass at each step. Approximately 200 to 250 μg ^{9}Be carrier solution was added to a sample weight of ~50 g to enable appropriate sample size and isotope ratio for a later measurement. Beryllium was then extracted and purified using ion exchange column chromatography. The final steps before measurement, including pressing and loading of the samples into cathodes, were performed at the Ion Beam Laboratory at ETH Zurich, Hönggerberg where the samples were measured at the LIP 0.5 MV compact accelerator mass spectrometry (AMS) facility (Tandy).

Results were normalized to secondary in-house standards S2007N and S2010N with nominal values of $^{10}Be/^{9}Be = 28.1 \times 10^{-12}$ and $^{10}Be/^{9}Be = 3.3 \times 10^{-12}$, respectively. S2007N and S2010N have been calibrated with our new primary standard ICN 01-5-1. ICN 01-5-1 is produced by K. Nishiizumi and has a nominal $^{10}Be/^{9}Be$ value of 2.709×10^{-11} (Nishiizumi et al., 2007, Christl et al., 2013). Blank corrections were performed using an arithmetic mean of 14 ^{10}Be blanks with zero outliers measured at the Tandy facility in the period of 4 months before our last measurement was conducted (20 blanks with one outlier in a period of one year before measurement for sample NEQ/162 79). AMS measurements were performed in June and September 2017 (June 2018 for sample NEQ/162 79).

Calculation of ages

Subsequently cosmogenic exposure ages were computed from the $^{10}Be/^{9}Be$ ratios including analytical errors measured at the AMS facility. The "Cosmic Ray Exposure program" (CREp) code, which is accessible online via the URL http://crep.crpg.cnrs-nancy.fr (Martin et al., 2017), was used to calculate exposure ages from nuclide concentrations. This web-based computational tool was chosen because it utilizes a robust production rate calibration database set up by the Informal Cosmogenic-nuclide Exposure-age Database (ICE-D) project (http://calibration.ice-d.org). The database is continuously updated and compiles and aligns production rate calibration data published for a variety of locations globally (Martin et al., 2017). Parameters input into CREp include the ^{10}Be concentration in the samples (calculated from the measured ratios) with 1σ-error, sample location coordinates and altitude, topographic shielding, an assumed uniform rock sample density of 2.7 g cm-3 and the average sample thickness. We applied the Lifton-Sato-Dunai (LSD) theoretical scaling scheme (Lifton et al., 2014) for our age computation which uses analytical approximations to modelled cosmic ray particle fluxes giving specific atmospheric cross-sections for the ^{10}Be-nuclide and the other particles involved in the corresponding nuclear reactions (Martin et al., 2017). Another input scheme is the ERA-40 atmosphere model (Uppala et al., 2005) based on a 45 year spanning database of atmospheric pressures for any locations on earth. It gives a pressure distribution approximation necessary because atmospheric pressure has an impact on the local production rate of cosmogenic nuclides. The geomagnetic record Lifton 2016 VDM (Pavón-Carrasco et al., 2014; Laj et al., 2004; Ziegler et al., 2011) was chosen to account for variations in the earth's magnetic field in the past. We chose a global mean production rate because no production rate calibration data was available for the whole Asian continent (see full list of references on http://crep.crpg.cnrs-nancy.fr or Martin et al., 2017). We computed our ages on the 7th of June 2018.

Table S3-1: Boulder exposure ages – results

Sample #	River	Lat [°]	Lon [°]	Alt. [m a.s.l.] (1)	Sample thickness [cm]	Shielding	$^{10}Be/^{9}Be$ ratio [10^{-14}]	1σ analytical error of ratio [%]	Sample weight [g]	Amount of carrier (µg) (2)	^{10}Be [at/g] (3)	1σ AMS final error [%] (3)	Exposure age ± 1σ [ka BP] (4)
NEQ/161 01	SUNKOSHI	27.729	85.779	674	2.0	0.86	3.70	8.8	21.381	201.6	1.67×10^4	13.9	4.98 ± 0.65
NEQ/161 02	SUNKOSHI	27.728	85.779	672	3.0	0.93	1.02	15.3	40.957	256.4	9.18×10^2	95.8	maximum 0.49 (5)
NEQ/161 03	SUNKOSHI	27.724	85.778	686	6.5	0.95	14.83	5.1	34.978	201.9	5.28×10^4	5.6	13.28 ± 0.96
NEQ/162 44	TRISHULI	27.856	85.070	441	3.0	0.99	2.26	10.5	22.521	256.6	1.10×10^4	19.1	3.48 ± 0.67
NEQ/162 45	TRISHULI	27.856	85.069	440	3.0	0.99	6.48	6.6	43.087	201.7	1.69×10^4	8.5	5.22 ± 0.46
NEQ/162 46	TRISHULI	27.856	85.069	445	3.0	0.99	4.69	7.8	33.040	202.4	1.49×10^4	11.1	4.64 ± 0.54
NEQ/162 47	TRISHULI	27.856	85.068	445	2.5	0.99	4.81	7.5	41.518	257.1	1.64×10^4	9.7	5.05 ± 0.49
NEQ/162 58	TRISHULI	28.009	85.184	679	4.5	0.96	6.96	6.8	58.751	197.7	1.32×10^4	8.5	3.63 ± 0.35
NEQ/162 59	TRISHULI	28.009	85.184	680	4.0	0.95	2.15	10.8	37.292	200.9	4.03×10^3	26.2	1.06 ± 0.29
NEQ/162 60	TRISHULI	27.970	85.183	618	2.0	0.97	8.08	5.5	60.322	202.8	1.57×10^4	6.8	4.35 ± 0.37
NEQ/162 61	TRISHULI	27.969	85.182	609	1.5	0.97	4.26	7.1	40.426	254.7	1.44×10^4	9.7	4.01 ± 0.43
NEQ/162 66a	TRISHULI	27.970	85.180	630	2.0	0.98	9.52	5.7	61.306	201.7	1.85×10^4	6.7	4.82 ± 0.49 (6)
NEQ/162 66b	TRISHULI	27.970	85.180	630	2.0	0.98	4.25	10.6	41.450	304.8	1.74×10^4	13.0	
NEQ/162 67	TRISHULI	27.971	85.180	632	2.5	0.98	10.50	5.3	61.830	203.3	2.06×10^4	6.1	5.46 ± 0.38
NEQ/162 79	SUNKOSHI, Balephi Khola	27.735	85.780	683	1.5	0.96	6.65	14.3	39.027	251.1	2.46×10^4	16.7	6.23 ± 0.92
NEQ/162 80	SUNKOSHI	27.734	85.783	695	1.5	0.95	11.93	5.1	41.942	255.9	4.49×10^4	5.6	10.96 ± 0.73
NEQ/162 98	SUNKOSHI, Balephi Khola	27.741	85.777	693	1.5	0.90	5.05	8.2	40.199	256.3	1.79×10^4	10.3	4.97 ± 0.51

(1) elevation of sampling point (2) 6.616×10^{19} atoms ^{9}Be per gram carrier

(3) after blank correction: $1.36 \times 10^5 \pm 2.44 \times 10^4$ ^{10}Be atoms n = 14 blank measurements over 4 months in same laboratory (except for NEQ/162 79 that was corrected for a blank contribution of $1.43 \times 10^5 \pm 2.77 \times 10^4$ ^{10}Be atoms, n = 20 blank measurements over 1 year in same laboratory)

(4) calculated with online version of CREp (Martin et al.2017) on 7.6.2018, see text for set parameters and production rate.

(5) not statistically different from blank, yields only a maximum concentration

(6) age was calculated using the mean ^{10}Be concentrations from duplicate measurements NEQ/162 66A and NEQ/162 66B

Boulders at Betrawati, Trishuli valley

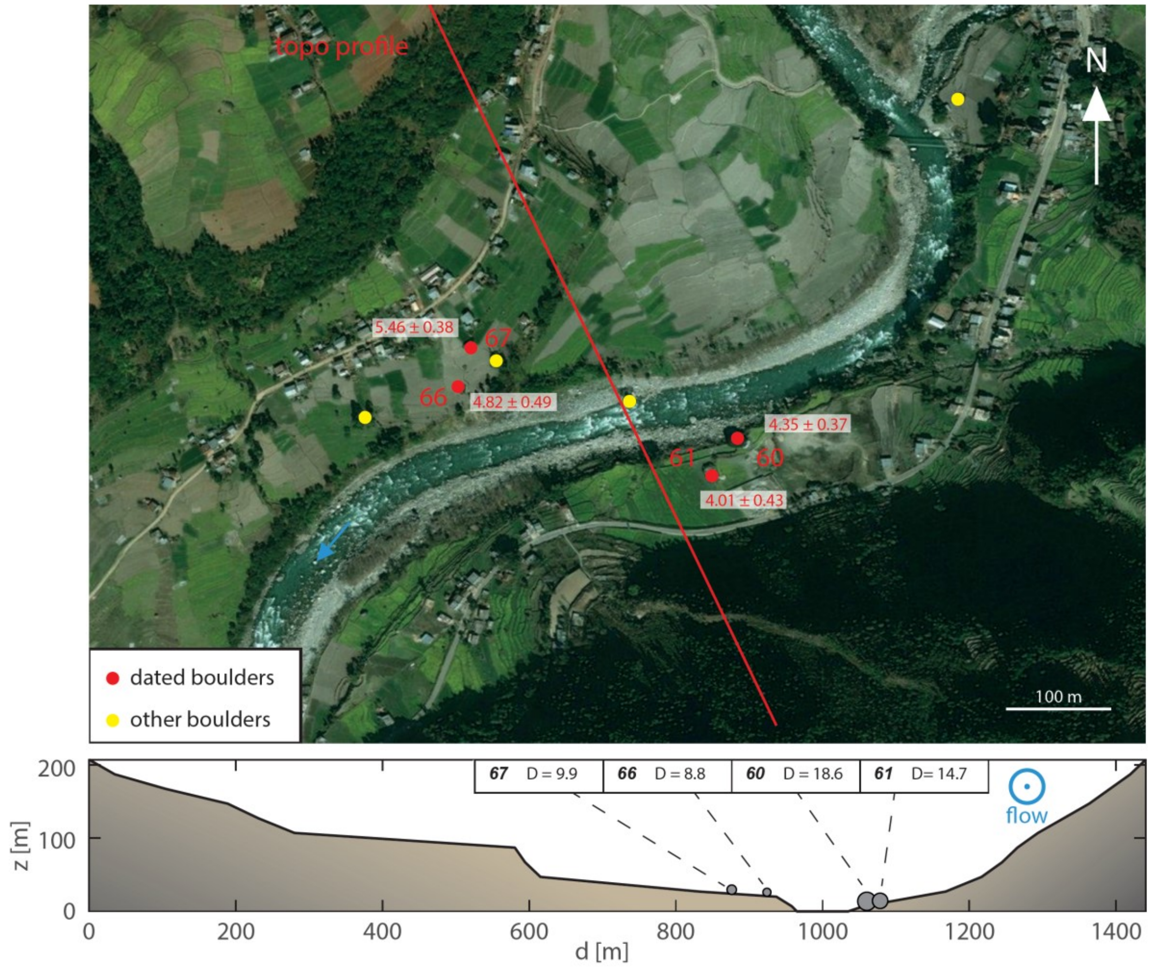

Figure S3-1: Top: Sample numbers are added without "NEQ/162…". Exposure ages are in ka BP. Zoom-out on tributary fan. Red line shows location of topo-profile (bottom). Bottom: boulder intermediate diameters in meters. Bing Maps. (n.d.). [Satellite Imagery for central Nepal], Retrieved June to November 2017, from https://www.bing.com/maps, © Microsoft. Topographic profile drawn from topographic maps (see S2).

Boulders south of Devighat, Trishuli valley

Figure S3-2: Top: Sample numbers are added without "NEQ/162…". Exposure ages are in ka BP. Middle: Zoom-out on tributary fan. Red line shows location of topo-profile (bottom). Bottom: boulder intermediate diameters in meters. Bing Maps. (n.d.). [Satellite Imagery for central Nepal], Retrieved June to November 2017, from https://www.bing.com/maps, © Microsoft. Topographic profile drawn from topographic maps (see S2).

Table S3-2: Exposure-dated moraine deposits in the central Himalayan study region – recalculated for comparison with boulder exposure ages in this study

(these ages are plotted in Figure 6)

	Isotope	Sample	Lat [dec°]	Lon [dec°]	Alt [masl]	Conc [at/g]	1s [at/g]	Shield. Corr	Density [g/cm^3]	Thickness [cm]	Landform allocation	Exposure age ± 1	
Finkel et al. (2003)	10Be	E5	27.89	86.82	4328	1143000	33000	0.99	2.7	2	Periche II glacial stage	23.17	± 1.22
	10Be	E6	27.89	86.82	4433	966000	23000	0.99	2.7	2	Periche II glacial stage	19.53	± 0.99
	10Be	E7	27.89	86.82	4310	973000	24000	0.99	2.7	2	Periche II glacial stage	20.66	± 0.97
	10Be	E29	27.9	86.87	4755	1319000	16000	0.99	2.7	2	Chhukung glacial stage	21.92	± 0.93
	10Be	E30	27.9	86.87	4837	71000	21000	0.99	2.7	2	Chhukung glacial stage	1.42	± 0.45
	10Be	E31	27.9	86.87	4812	697000	16000	0.99	2.7	2	Chhukung glacial stage	12.5	± 0.73
	10Be	E32	27.9	86.87	4773	53000	7000	0.99	2.7	2	Lobuche and historical glacial stage	1.08	± 0.16
	10Be	E37	27.9	86.87	4691	75000	21000	0.99	2.7	2	Lobuche and historical glacial stage	1.62	± 0.49
	10Be	E38	27.9	86.87	4718	8000	3000	0.99	2.7	2	Lobuche and historical glacial stage	0.16	± 0.06
	10Be	E39	27.91	86.88	5074	1714000	45000	0.99	2.7	2	Periche I glacial stage	24.06	± 1.26
	10Be	E46	27.91	86.87	5047	1606000	48000	0.99	2.7	2	Periche I glacial stage	22.99	± 1.20
	10Be	E59	27.92	86.89	5324	694000	17000	0.99	2.7	2	Periche I glacial stage	10.22	± 0.54
	10Be	E61	27.91	86.89	5005	297000	22000	0.99	2.7	2	Thuklha glacial stage	5.49	± 0.38
	10Be	E62	27.91	86.88	4955	274000	11000	0.99	2.7	2	Thuklha glacial stage	5.25	± 0.29
	10Be	E63	27.91	86.88	5032	257000	15000	0.98	2.7	2	Thuklha glacial stage	4.87	± 0.34
	10Be	E73	27.91	86.81	4557	1047000	32000	0.98	2.7	2	Periche II glacial stage	19.99	± 1.03
	10Be	E79	27.92	86.81	4624	66000	16000	0.98	2.7	2	Chhukung glacial stage	1.47	± 0.39
	10Be	E80	27.92	86.81	4624	671000	31000	0.98	2.7	2	Chhukung glacial stage	13.16	± 0.85
	10Be	E81	27.92	86.81	4628	676000	26000	0.98	2.7	2	Chhukung glacial stage	13.22	± 0.78
	10Be	E82	27.92	86.81	4270	85000	10000	0.99	2.7	2	Lobuche and historical glacial stage	2.3	± 0.33
Schaefer et al. (2008)	10Be	Ny-9	28.185	85.935	4301	1005000	61280	0.978	2.7	1	Puluo 1 moraine	21.14	± 1.30
	10Be	Ny-10	28.183	85.933	4301	1576000	77230	0.978	2.7	2	Puluo 1 moraine	31.65	± 2.56
	10Be	Ny-12-1	28.168	85.933	4261	665400	29280	0.978	2.7	2.5	Puluo 2 moraine	15.2	± 0.94
	10Be	Ny-12-2	28.168	85.933	4261	655800	26230	0.978	2.7	2.5	Puluo 2 moraine	15.03	± 0.89
	10Be	Ny-13	28.168	85.933	4273	709500	51080	0.978	2.7	4	Puluo 2 moraine	16.24	± 1.3
	10Be	Ny-14-1	28.168	85.933	4265	475800	26170	0.978	2.7	6.1	Puluo 2 moraine	11.52	± 0.78
	10Be	Ny-14-2	28.168	85.933	4265	620000	24800	0.978	2.7	6.1	Puluo 2 moraine	14.73	± 0.85
	10Be	NAI-1	28.317	86.05	4289	928800	55790	0.974	2.7	3	youngest Naisa moraine	20.26	± 1.32
	10Be	NAI-2	28.317	86.05	4308	1061000	33940	0.974	2.7	3.9	youngest Naisa moraine	22.28	± 1.13
	10Be	NAI-3	28.317	86.05	4343	861800	46780	0.974	2.7	5.9	youngest Naisa moraine	18.97	± 1.27
Abramowski et al. (2003)	10Be	MK41	28.3	84.5	3900	249000	22000	1	2.7	4	neoglacial	7.26	± 0.65
	10Be	MK42	28.3	84.5	3900	101000	15000	1	2.7	4	neoglacial	3.34	± 0.51
	10Be	MK43	28.3	84.5	3900	180000	14000	1	2.7	4	neoglacial	5.59	± 0.41
	10Be	MK44	28.3	84.5	3900	154000	24000	1	2.7	4	neoglacial	4.93	± 0.69
	10Be	MK45	28.3	84.5	3900	178000	34000	1	2.7	4	neoglacial	5.54	± 0.89
	10Be	MK52	28.3	84.5	3550	484000	35000	1	2.7	4	MIS 2	15.87	± 1.27
	10Be	MK54	28.3	84.5	3550	895000	78000	1	2.7	4	MIS 2	26.8	± 2.52
	10Be	MK55	28.3	84.5	3550	510000	55000	1	2.7	4	MIS 2	16.64	± 1.79
	10Be	MK73	28.3	84.5	3260	470000	56000	1	2.7	4	lateglacial	17.97	± 2.09
	10Be	MK74	28.3	84.5	3260	435000	44000	1	2.7	4	lateglacial	16.76	± 1.74
	10Be	MK75	28.3	84.5	3260	450000	39000	1	2.7	4	lateglacial	17.28	± 1.61
	10Be	LT22	28.2	85.6	4150	903000	45000	0.994	2.7	3	Kyangchen Gomba high	20.68	± 1.18
	10Be	LT23	28.2	85.6	4156	844000	32000	0.993	2.7	1	Kyangchen Gomba high	19.25	± 1.11
	10Be	LT24	28.2	85.6	4156	893000	47000	0.988	2.7	2	Kyangchen Gomba high	20.4	± 1.23
	10Be	LT26	28.2	85.6	4154	735000	36000	0.988	2.7	2	Kyangchen Gomba high	17.26	± 1.15
	10Be	LT32	28.2	85.6	3853	431000	17000	0.973	2.7	2.5	Kyangchen Gomba end	12.64	± 0.82
	10Be	LT33	28.2	85.6	3851	403000	16000	0.964	2.7	2.5	Kyangchen Gomba end	11.89	± 0.77
	10Be	LT35	28.2	85.6	3846	458000	21000	0.982	2.7	1	Kyangchen Gomba end	13.09	± 0.86
	10Be	LT36	28.2	85.6	3846	192000	8000	0.926	2.7	2	Kyangchen Gomba end	6.33	± 0.35
	10Be	LT61	28.2	85.5	3523	129000	8000	0.963	2.7	1.5	Langtang stage	5.13	± 0.36
	10Be	LT63	28.2	85.5	3525	134000	7000	0.948	2.7	1	Langtang stage	5.33	± 0.32
Gayer et al. (2006)	3He	GA24	28.232	85.188	4490	1.7E+07	1290000	0.99	2.7	2.5	M3 moraine stage	11.04	± 1.10
	10Be	GA24	28.232	85.188	4490	317800	32400	0.99	2.7	2.5	M3 moraine stage	6.94	± 0.65
	3He	GA26	28.232	85.188	4500	2E+07	2630000	0.99	2.7	2.5	M1-2 moraine stage	12.62	± 1.77
	3He	GA45	28.229	85.189	4410	1.7E+07	2360000	0.95	2.7	2.5	M3 moraine stage	11.68	± 1.71
	3He	GA54	28.227	85.188	4434	1.5E+07	1360000	0.98	2.7	2.5	M3 moraine stage	10	± 1.25
	10Be	GA54	28.227	85.188	4434	357400	24100	0.98	2.7	2.5	M3 moraine stage	7.93	± 0.65
	3He	GA55	28.227	85.188	4446	2.1E+07	6830000	0.98	2.7	2.5	M3 moraine stage	13.62	± 4.00
	10Be	GA55	28.227	85.188	4446	587800	65700	0.98	2.7	2.5	M3 moraine stage	12.6	± 1.39
	3He	GA56	28.225	85.192	4288	1.9E+07	1680000	0.96	2.7	2.5	M4-5 moraine stage	13.4	± 1.6
	3He	MAI12	28.216	85.196	3760	4510000	1080000	0.92	2.7	2.5	M3 moraine stage	5.13	± 1.12
	3He	MAI15	28.216	85.195	3800	5080000	1340000	0.92	2.7	2.5	M3 moraine stage	5.53	± 1.28
	3He	MAI17	28.23	85.189	4530	1.2E+07	1600000	0.99	2.7	2.5	M4-5 moraine stage	7.52	± 1.12
Pratt-Sitaula et al. (2011)	10Be	CRN-222	28.6756	84.0551	4614	1015000	33000	0.993	2.65	1.5	Kicho	18.37	± 1.04
	10Be	CRN-223	28.6756	84.0551	4614	949000	25000	0.987	2.65	1.5	Kicho	17.38	± 0.97
	10Be	CRN-224	28.6805	84.0585	4660	1101000	39000	0.994	2.65	2	Kicho	19.37	± 1.08
	10Be	CRN-225	28.6792	84.0568	4661	1010000	27000	0.996	2.65	2	Kicho	17.93	± 0.98
	10Be	CRN-226	28.6882	84.0234	4500	524000	16000	0.969	2.65	3	Syaktan	11.1	± 0.54
	10Be	CRN-227	28.6882	84.0234	4500	611000	17000	0.969	2.65	3	Syaktan	12.78	± 0.75
	10Be	CRN-228	28.6944	84.0253	4744	588000	16000	0.962	2.65	3	Syaktan	11.14	± 0.52
	10Be	CRN-229	28.6944	84.0253	4744	541000	16000	0.962	2.65	3	Syaktan	10.43	± 0.55
	10Be	CRN-246	28.4008	84.2291	3960	659000	19000	0.956	2.7	3	Midim	17.69	± 1.00
	10Be	CRN-247	28.4008	84.2291	3960	667000	31000	0.956	2.7	3	Midim	17.87	± 1.16
	10Be	CRN-248	28.4008	84.2291	3960	627000	31000	0.956	2.7	3	Midim	16.93	± 1.15
	10Be	CRN-249	28.4003	84.2303	3910	618000	18000	0.956	2.7	3	Midim	17.11	± 0.96
	10Be	CRN-250	28.4003	84.2303	3910	632000	17000	0.956	2.7	3	Midim	17.45	± 0.98
	10Be	CRN-251	28.4083	84.2719	3610	604000	16000	0.97	2.7	2.5	Khudi	19.07	± 1.01
	10Be	CRN-252	28.4083	84.2719	3625	626000	20000	0.97	2.7	2	Khudi	19.46	± 1.06
	10Be	CRN-253a	28.4083	84.2719	3632	598000	16000	0.97	2.7	2.5	Khudi	18.71	± 1.02
	10Be	CRN-254	28.4083	84.2719	3640	594000	18000	0.97	2.7	1.5	Khudi	18.39	± 1.03
	10Be	CRN-433	28.4735	84.3172	4009	374000	10000	0.917	2.75	1	Danfe	10.76	± 0.53
	10Be	CRN-434	28.4739	84.3165	4057	380000	10000	0.945	2.75	2	Danfe	10.45	± 0.54
	10Be	CRN-435	28.4741	84.3163	4068	401000	10000	0.945	2.75	1	Danfe	10.84	± 0.52
	10Be	CRN-437	28.4784	84.3126	4213	456000	12000	0.962	2.75	2	Danfe	11.16	± 0.52
	10Be	CRN-438	28.4784	84.3126	4215	429000	9000	0.962	2.75	1	Danfe	10.59	± 0.51
	10Be	CRN-439	28.4789	84.3116	4249	467000	12000	0.98	2.75	1	Danfe	11.02	± 0.51
	10Be	CRN-440	28.4734	84.3178	3978	386000	10000	0.916	2.75	2	Danfe	11.2	± 0.52

zero erosion rate assumed for all samples; samples were calculated with worldwide mean SLHL production rates (weighted mean, ^{10}Be: 4.08 +/- 0.23 at/g/yr ^{3}He: 121.14 +/- 11.53 at/g/yr) with CREp web-based calculator (see Martin et al. 2017 for further details) on Fri Sep 07 2018

References

Abramowski, U., 2004. The use of 10Be surface exposure dating of erratic boulders in the reconstruction of the late Pleistocene glaciation history of mountainous regions, with examples from Nepal and Central Asia.

Christl, M., Vockenhuber, C., Kubik, P., Wacker, L., Lachner, J., Alfimov, V. and Synal, H.-A., 2013. The ETH Zurich AMS facilities: Performance parameters and reference materials. Nuclear Instruments and Methods in Physics Research Section B: Beam Interactions with Materials and Atoms, 294: 29-38.

Dhital, M.R., 2015. Geology of the Nepal Himalaya: regional perspective of the classic collided orogen. Springer.

Dunai, T.J., 2010. Cosmogenic Nuclides: Principles, concepts and applications in the Earth surface sciences. Cambridge University Press.

Finkel, R.C., Owen, L.A., Barnard, P.L. and Caffee, M.W., 2003. Beryllium-10 dating of Mount Everest moraines indicates a strong monsoon influence and glacial synchroneity throughout the Himalaya. Geology, 31(6): 561-564.

Gayer, E., Lavé, J., Pik, R. and France-Lanord, C., 2006. Monsoonal forcing of Holocene glacier fluctuations in Ganesh Himal (Central Nepal) constrained by cosmogenic 3He exposure ages of garnets. Earth and Planetary Science Letters, 252(3-4): 275-288.

Ivy-Ochs, S.D., 1996. The Dating of Rock Surfaces Using in Situ Produced 10 Be, 26 Al and 36 Cl: With Examples from Antarctica and the Swiss Alps. Diss. Naturwiss., Doctoral Thesis Thesis, ETH Zurich.

Ivy-Ochs, S. and Kober, F., 2008. Surface exposure dating with cosmogenic nuclides. Quaternary Science Journal, 57(1-2): 179-209.

Laj, C., Kissel, C. and Beer, J., 2004. High Resolution Global Paleointensity Stack Since 75 kyr (GLOPIS-75) Calibrated to Absolute Values. Timescales of the Paleomagnetic Field: 255-265.

Martin, L., Blard, P.-H., Balco, G., Lavé, J., Delunel, R., Lifton, N. and Laurent, V., 2017. The CREp program and the ICE-D production rate calibration database: A fully parameterizable and updated online tool to compute cosmic-ray exposure ages. Quaternary geochronology, 38: 25-49.

Nishiizumi, K., Imamura, M., Caffee, M.W., Southon, J.R., Finkel, R.C. and McAninch, J., 2007. Absolute calibration of 10 Be AMS standards. Nuclear Instruments and Methods in Physics Research Section B: Beam Interactions with Materials and Atoms, 258(2): 403-413.

Norton, K.P., von Blanckenburg, F., Schlunegger, F., Schwab, M. and Kubik, P.W., 2008. Cosmogenic nuclide-based investigation of spatial erosion and hillslope channel coupling in the transient foreland of the Swiss Alps. Geomorphology, 95(3): 474-486.

Pavón-Carrasco, F.J., Osete, M.L., Torta, J.M. and De Santis, A., 2014. A geomagnetic field model for the Holocene based on archaeomagnetic and lava flow data. Earth and Planetary Science Letters, 388: 98-109.

Pratt-Sitaula, B., Burbank, D.W., Heimsath, A. and Ojha, T., 2004. Landscape disequilibrium on 1000–10,000 year scales Marsyandi River, Nepal, central Himalaya. Geomorphology, 58(1): 223-241.

Schaefer, J.M., Oberholzer, P., Zhao, Z., Ivy-Ochs, S., Wieler, R., Baur, H., Kubik, P.W. and Schlüchter, C., 2008. Cosmogenic beryllium-10 and neon-21 dating of late Pleistocene glaciations in Nyalam, monsoonal Himalayas. Quaternary Science Reviews, 27(3): 295-311.

Shrestha, S.B., Shrestha, J.N., Sharma, S.R., 1986. Geological map of central Nepal.

Uppala, S.M., Kållberg, P., Simmons, A., Andrae, U., Bechtold, V.d., Fiorino, M., Gibson, J., Haseler, J., Hernandez, A. and Kelly, G., 2005. The ERA-40 re-analysis. Quarterly Journal of the royal meteorological society, 131(612): 2961-3012.

Von Blanckenburg, F., Belshaw, N. and O'Nions, R., 1996. Separation of 9Be and cosmogenic 10Be from environmental materials and SIMS isotope dilution analysis. Chemical Geology, 129(1-2): 93-99.

Von Blanckenburg, F., Hewawasam, T. and Kubik, P.W., 2004. Cosmogenic nuclide evidence for low weathering and denudation in the wet, tropical highlands of Sri Lanka. Journal of Geophysical Research: Earth Surface, 109(F3).

Ziegler, A.D., Wasson, R.J., Bhardwaj, A., Sundriyal, Y., Sati, S., Juyal, N., Nautiyal, V., Srivastava, P., Gillen, J. and Saklani, U., 2014. Pilgrims, progress, and the political economy of disaster preparedness-the example of the 2013 Uttarakhand flood and Kedarnath disaster. Hydrological Processes, 28(24): 5985-5990.